Journal of Colloid and Interface Science 466 (2016) 247–253

Contents lists available at ScienceDirect

Journal of Colloid and Interface Science

journal homepage: www.elsevier.com/locate/jcis

Dynamic and structural correlations in nanocomposites of silica with modified surface and carboxylated nitrile rubber

Renata L. Sala [a], Tatielih P. Oliveira Xavier [b], Tiago Venâncio [b], Tatiane Moraes Arantes [c], Caio M. Paranhos [b], Emerson R. Camargo [a,*]

[a] LIEC – Interdisciplinary Laboratory of Electrochemistry and Ceramics, Department of Chemistry, UFSCar – Federal University of São Carlos, Rod. Washington Luis km 235, CP 676, 13565-905 São Carlos, SP, Brazil
[b] Department of Chemistry, UFSCar – Federal University of São Carlos, Rod. Washington Luis km 235, CP 676, 13565-905 São Carlos, SP, Brazil
[c] Chemistry, Federal Institute of Education, Science and Technology Goiano, Sul Goiânia Avenue, km 1, Zona Rural, 75901-970 Rio Verde, GO, Brazil

GRAPHICAL ABSTRACT

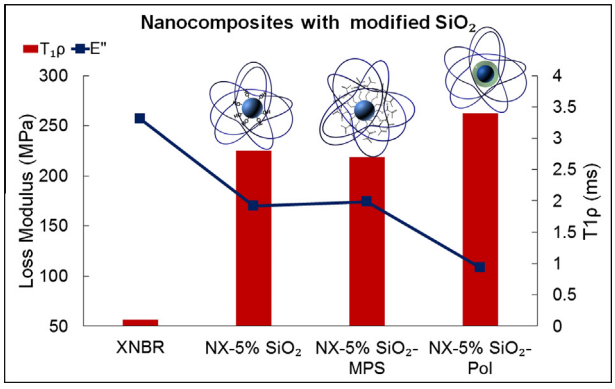

ARTICLE INFO

Article history:
Received 28 September 2015
Revised 12 December 2015
Accepted 17 December 2015
Available online 17 December 2015

Keywords:
Polymer–matrix composites
Thermomechanical properties
Solid state NMR

ABSTRACT

Distinct affinities between the organic and inorganic phases were observed in nanocomposites prepared through a colloidal route with carboxylated nitrile rubber and modified silica nanoparticles, which resulted in variable mechanical properties and improved thermal stability. Nanoparticles with modified surface affected the macromolecular arrangements of the elastomeric matrix, changing the final mechanical behavior of the nanocomposite, which could be predicted by the spin–lattice relaxation time measured by solid-state NMR. It was also possible to identify how each different nanoparticle affected the molecular dynamic of nanocomposite, correlating the dynamic-mechanical analysis with the NMR data of the saturated carbons of the elastomer.

1. Introduction

Among the organic/inorganic hybrid materials, polymeric nanocomposites with silica have attracted a great attention due their improved and versatile properties. The pioneer and largest application of SiO_2 nanoparticles was as fillers in tires aiming to increase their wet grip, rolling and mechanical resistance [1].

* Corresponding author.
E-mail addresses: renata.lang89@gmail.com (R.L. Sala), tatielih.pdo@gmail.com (T.P. Oliveira Xavier), t_venancio@yahoo.com (T. Venâncio), tmarantes@yahoo.com.br (T.M. Arantes), paranhos@ufscar.br (C.M. Paranhos), camargo@ufscar.br (E.R. Camargo).

http://dx.doi.org/10.1016/j.jcis.2015.12.028
0021-9797/

During the last few years, silica showed to be very versatile, becoming essential for many applications, such as coatings [2], flame retardants [3], optical devices [4], electronic matrices [5], sensors [6] and drug delivery [7]. Silane agents, on the other hand, have been widely used to modify the surface of nanoparticles and have gained prominence promoting interfacial adhesive strength between particles and macromolecules due to changes in the chemical reactivity and hydrophobicity of nanoparticles [8–10]. Specifically, the carboxylated nitrile rubber (XNBR) latex exhibits several advantages since the presence of colloids in the aqueous suspension of nanoparticles facilitates their incorporation by the polymeric matrix. Additionally, XNBR contains carboxyl groups that interact strongly with fillers resulting in better mechanical properties [11–14].

To investigate the role played by SiO_2 nanoparticles in the XNBR matrix, we synthesized modified nanoparticles with silane coupling agents followed by the formation of a hydrophobic shell with controlled thickness. Solid-state NMR was used to investigate how these modified nanoparticles affected the interface between organic and inorganic phases [15,16]. Using the technique of cross polarization (CP) in NMR, it was possible not only to overcome the difficulty to acquire spectra of dilute nuclei, such as ^{13}C and ^{29}Si, but also to get important information about the dynamics of the nanocomposite structure. The dynamics can be evaluated by CP approach through the measurement of the spin–lattice relaxation time in the rotating frame ($T_{1\rho}$) and the contact time between both nuclei involved in the process (T_{IS}) [17]. The magnitude of these parameters is dependent on the magnetization transfer of an abundant spin nucleus (I), such as hydrogen, to another less abundant spin (S), as ^{13}C. When this technique is used in combination with Magic Angle Spinning (MAS) and high-power decoupling, it provides high-resolution spectra for solids, being possible to study a very specific site of the polymer structure and its environment. Complementally, thermogravimetric (TGA) and dynamic mechanical analyzes (DMA) were performed to evaluated the aspects of the hybrid materials structures that interfere in the final materials performance and applications [18].

2. Experimental section

2.1. Synthesis of the nanoparticles and nanocomposites

The nanoparticles and nanocomposites were synthesized as previously described [19,20]. Colloidal silica nanoparticles (SiO_2) were prepared at room temperature through the hydrolysis and controlled condensation of 26.4 mmol of tetraethyl orthosilicate (TEOS, 98%, Aldrich, USA) in a mixture of 25 mL of distilled water, 70 mL of absolute ethanol and 0.51 mol of NH_3 from an aqueous solution (30%, analytical grade, Synth, Brazil) under stirring for 24 h. The modified nanoparticles were synthesized by adding the 3-(trimethoxysilyl)propyl methacrylate (MPS) coupling agent (98%, Aldrich, USA) into the suspension of unmodified silica (SiO_2-MPS). The core/shell systems (SiO_2-Pol) were prepared by applying the precipitation co-polymerization of styrene (St, >99%, Aldrich, EUA) and divinylbenzene (DVB, 80%, Aldrich, EUA) in the presence of azobisisobutyronitrile (AIBN, DuPont, Brazil), polyvinylpyrrolidone (Aldrich, EUA) and anhydrous ethanol under stirring for 5 h at 60° C.

Nanocomposites (thereafter referred to as NX) films were prepared by the colloidal route, which involves the mixture of commercial polymer latex of XNBR (43.7% of solids containing 25% of acrylonitrile, Nitriflex, Brazil) with the colloidal silica nanoparticles. Aqueous dispersions of pure SiO_2, SiO_2-MPS and SiO_2-Pol nanoparticles were prepared in the presence of 0.1 mol L^{-1} of sodium dodecyl sulfate (SDS) to improve the nanoparticle dispersion in the XNBR latex, which was homogenized for 1 h and dried in Petri dishes at 50 °C.

2.2. Methods of characterization

The morphology and size of the SiO_2-MPS nanoparticles were characterized by scanning electron microscopy (SEM) in a JEOL JSM-5600LV operating at 20 kV, and the SiO_2-Pol images were collect using a TECNAI F20 field emission HRTEM operating at 200 kV. Solid-state NMR spectra were recorded in a Bruker Avance III spectrometer operating at a magnetic field of 9.4 T Oxford, which has a related frequency of 400 MHz for the hydrogen-1 nucleus. Analyzes were performed using techniques of cross polarization with rotation under the magic angle and total sideband suppression (CPTOSS) at room temperature (23 °C). Values of $T_{1\rho}$ were estimated by running the CP with variable contact time pulse sequence by using the recycle delay of 7 s, variable contact time (10 μs to 50 ms) and the spinning speed on magic angle of 5 kHz. The data processing to determine the $T_{1\rho}$ was done by using the treatment proposed by Kolodziejski and Klinowski [17] for heterogeneous samples, adjusting the data points according to Eq. (1), where I_0 is the absolute amplitude, T_{IS} is a CP time constant related to the dipolar interaction between the I (^1H) and S (^{13}C) spins of specific functional groups, and $1/T_{IS}$ is the CP rate constant that depends on the number and mobility of the protons. Dynamic mechanical properties of the nanocomposites were measured in a DMA 2980 equipment, TA instruments Q800. An oscillatory shear deformation at the constant frequency of 1 Hz with the conditions of 25 μm of amplitude, heating rate of 3 °C/min in the range of −60 °C to 30 °C was applied to analyze the samples with length of 50 mm and width of 10 mm. The thermal degradation of nanocomposites was evaluated by the thermoanalyzer (TGA), TG 209 F1 from Netzch. The samples were examined under an O_2 flow rate of 10 mL min^{-1}, at a heating rate of 10 °C min^{-1} and in the range of 25–900 °C.

$$I(\tau) = I_0(1 - T_{IS}/T_{1\rho}(I))^{-1}[\exp(-\tau/T_{1\rho}(I) - \exp(\tau/T_{IS})] \quad (1)$$

3. Results and discussion

Unmodified SiO_2 nanoparticles were synthesized hydrolyzing TEOS with a basic catalyst in a defined amount of H_2O/ethanol [19,20], while the MPS coupling agent was grafted on the nanoparticles to react with the silanol groups of SiO_2, resulting in spherical nanoparticles (SiO_2-MPS) of 250 nm with sharp size distribution (Fig. 1a). The MPS added polymerizable vinyl groups on the surface of nanoparticles, which acted as seeds for the co-polymerization between the DVB crosslinker and styrene in the presence of a stabilizer. This optimized procedure allowed the synthesis of monodisperse hybrid nanoparticles of SiO_2-Pol with polymeric shells of 50 nm (Fig. 1b) [21].

The absence of any ^{13}C solid state NMR signal from the methoxy carbon around 50 ppm in the SiO_2-MPS spectrum of Fig. 1 indicates that the MPS was bonded to the surface of nanoparticles [2,22]. The signals at 8, 17 and 22 ppm are related to methylene carbons from MPS, as well as the signals at 124.2, 136.8 and 168.3 ppm are attributed to the methacrylate group (see Table 1). The spectrum of the SiO_2-Pol shows signals of the methyl (17 ppm) and methylene (30 ppm) carbons of commercial DVB and a peak of the polymer shell backbone at 41 ppm. Moreover, the polymerization of styrene with DVB in the polymeric shell around the nanoparticles resulted in linear and branched macromolecules, remaining some residual vinyl groups of the DVB, as indicated by the peaks at 138 and 113 ppm [23,24]. The signals of less shielded carbons at

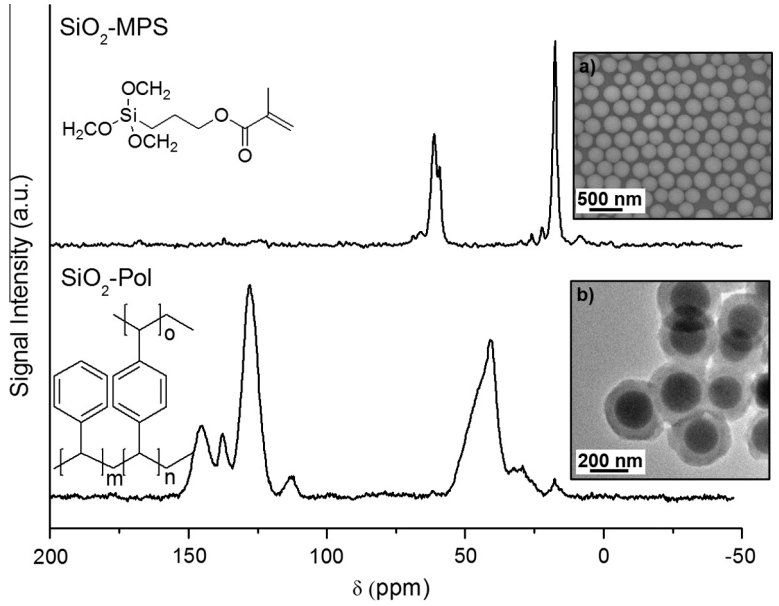

Fig. 1. ^{13}C CPTOSS NMR spectra of SiO_2 modified with MPS silane agent and with the polymer shell of styrene–divinylbenzene (Pol). (a) SEM image of SiO_2-MPS; and (b) HRTEM of SiO_2-Pol.

128 and 146 ppm belong to the phenyl ring and to the carbon attached directly to the vinyl group [23,24].

The peaks observed in the ^{13}C solid state NMR spectra of the nanocomposites in Fig. 2 are mainly related to butadiene (B), 1,2-butadiene (V) and acrylonitrile (A) units [25]. The spectra are quite similar, but there are some additional peaks in the spectra of the nanocomposites related to SDS surfactant (Table 2). It is important to note that the SiO_2-MPS and SiO_2-Pol nanoparticles modified the region related to saturated carbons of the elastomer, but unaffected the region of unsaturated carbons.

Both $T_{1\rho}$ and T_{IS} parameters were determined simultaneously and indirectly fitting the intensity $I(\tau)$ of the ^{13}C NMR signal in function of the contact time (τ) according to Eq. (1). The parameter $T_{1\rho}$ provides information about the molecular mobility, phase dispersion and homogeneity of the organic fraction in nanocomposites. The existence of rigid domains decreases its magnitude, which offers some insights about the interaction between the organic and inorganic components [26–28]. Fig. 3a shows the experimental decay curves of all samples in the region of unsaturated carbons. Their similar $T_{1\rho}$ values indicate that the nanoparticles did not affect the local mobility of the unsaturated carbons. On the other hand, the increasing of $T_{1\rho}$ related to saturated carbons of the nanocomposites (from 30 to 40 ppm) are different when compared to pure XNBR (Fig. 3b). These evident differences in $T_{1\rho}$ magnitude, which are related to changes in the local mobility of the macromolecules, show the existence of heterogeneities in

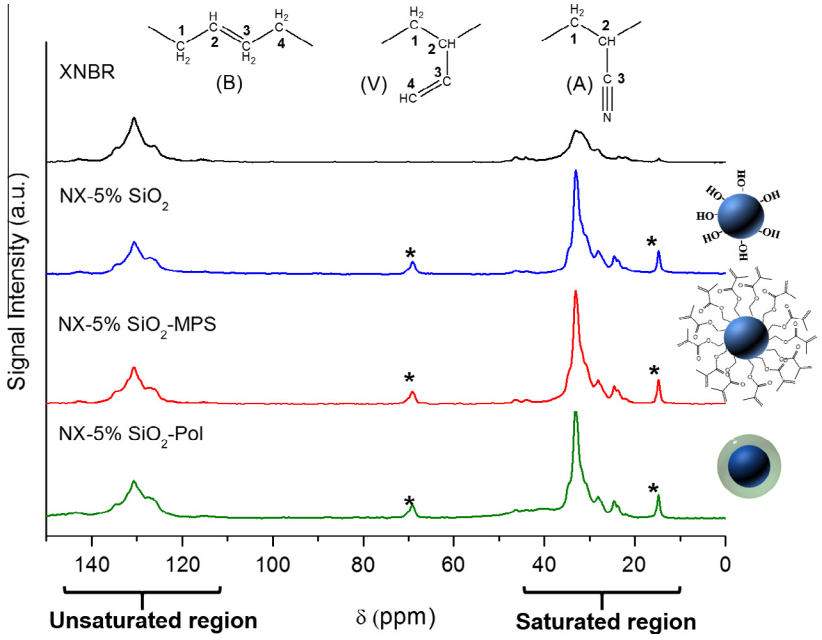

Fig. 2. ^{13}C CPTOSS NMR spectra of pure XNBR (composed by three major units: butadiene (B), 1,2-butadiene (V) and acrylonitrile (A) and nanocomposites with 5% of modified silica nanoparticles (NX-5% SiO_2, NX-5% SiO_2-MPS and NX-5% SiO_2-Pol).

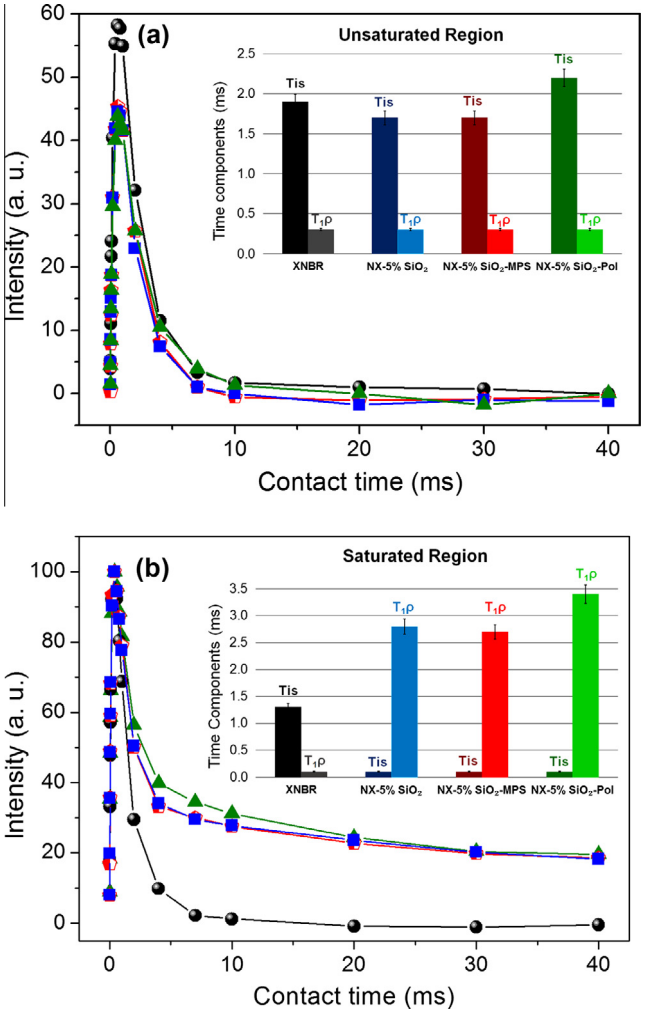

Fig. 3. Kinetic cross polarization curves for the unsaturated (a) (~150 ppm) and saturated (b) (~30 ppm) regions of XNBR, NX-5% SiO_2, NX-5% SiO_2-MPS and NX-5% SiO_2-Pol. Inset shows the $T_{1\rho}$ and T_{IS} parameters for all systems calculated by Eq. (1).

the nanocomposites not observed in pure XNBR [26,29,30]. Films of pure XNBR showed the lowest value of $T_{1\rho}$ in the region of saturated carbons, probably due to the presence of intermolecular and intramolecular interactions promoted by the carboxylate groups. However, the presence of SiO_2-Pol led to the highest value of $T_{1\rho}$, which can be related to the contribution of the polymer shell with a mobile character. The polymeric groups of the shell may have interacted preferably with the saturated aliphatic portion of XNBR, increasing its local mobility. Moreover, The SiO_2-MPS nanoparticles slightly lowered the $T_{1\rho}$ value when compared to the SiO_2, which means similar macro arrangements of the macromolecules around these two nanoparticles.

Although the surface of SiO_2 were modified to enhance the nanoparticle–polymer interaction, especially with the functional groups of the XNBR [31], only the region of saturated carbons in the nanocomposites were modified. It means that this region has more influence on structural and mechanical properties of nanocomposites than the adhesion interface promoted by specific functional groups of elastomers with the modified nanoparticles. The parameter T_{IS}, on the other hand, is associated with the dipolar interaction between the molecular chains [17,26]. The T_{IS} value from the region of saturated carbons of pure XNBR was higher than for nanocomposites and could be attributed to the stronger interaction among their carboxylated groups. The presence of nanoparticles intercalating the polymer decreased the dipolar coupling, which disfavored the polarization transfer, reducing the average dipolar coupling.

The thermal stability of conventional composites is proportional to the amount of SiO_2 nanoparticles when the degradation mechanism is unchanged. It occurs because the particles act as a simple thermal insulators and barriers to the diffusion of volatiles during the pyrolysis [3,32,33]. On the other hand, Liu et al. [34] observed an additional gain in thermal stability of nanocomposites of polyimide with up to 9% of SiO_2 due to changes in the degradation mechanism related to attractive forces between the polymer and the siloxanes and silanols from nanoparticles. Therefore, data from the thermal analysis can shed light on the interaction between the nanoparticles and the organic component in polymer based nanocomposites. Fig. 4a shows the TGA curves of the nanocomposites with different amounts of modified SiO_2. Although similar, their heating profiles are significantly different after 400 °C even for samples with the same amount of nanoparticles. This improved stability suggests an attractive interaction between the nanoparticles and the polymeric matrix. The first derivative of the thermograms (DTG) in Fig. 4b shows the degradation temperature increasing from 420 °C in the pure polymer to 427 and 426 °C for the nanocomposites with 1% and 5% of nanoparticles, respectively. However, the presence of coupling agents on the surface of silica did not influenced in this degradation temperature.

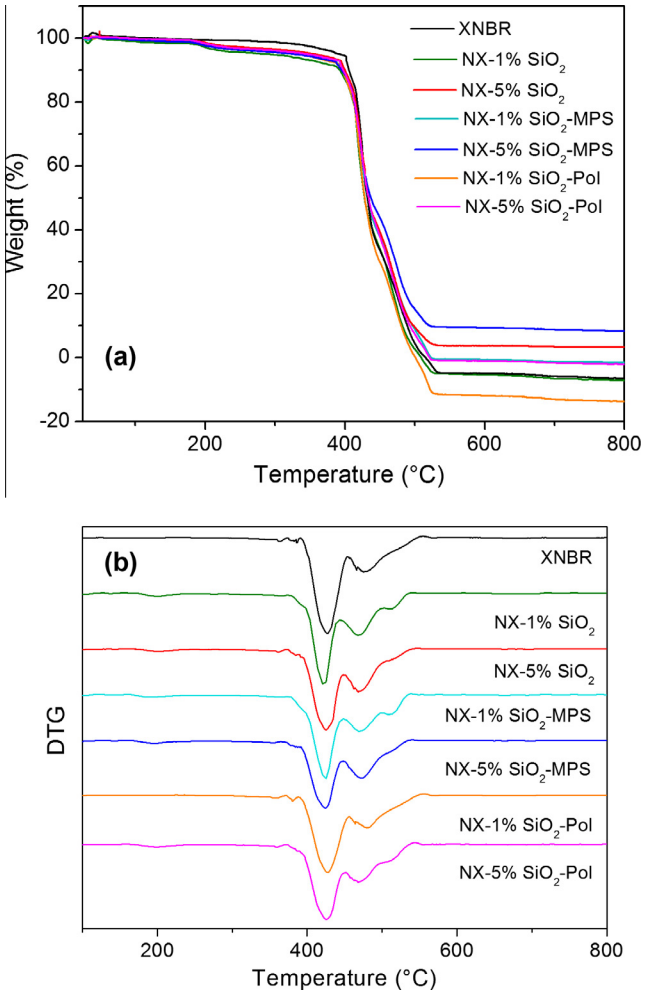

Fig. 4. Thermal degradation of pure polymer and nanocomposites with 1% and 5% of SiO_2, SiO_2-MPS and SiO_2-Pol (a). First derivative of thermograms to investigate the temperature range of maximum polymer degradation (b).

Table 1
^{13}C chemical shift values for the SiO_2-MPS and SiO_2-Pol nanoparticles.

SiO_2-MPS		SiO_2-Pol	
Structure	^{13}C chemical shift (ppm)	Structure	^{13}C chemical shift (ppm)
$SiCH_2$	8	$—CH_2CH_3$	17
$CH_3C═CH_2$	17	$—CH_2CH_3$	30
$SiCH_2CH_2$	22	Backbone CH/CH_2	41
CH_2O	67	$═CH_2$	113
$C═CH_2$	124	Aromatic (Ar)	128
$C═CH_2$	137	—CH═	138
$CH_2OC═O$	168	Ar-backbone	146

Table 2
^{13}C chemical shift values for XNBR and nanocomposites with 5% of SiO_2, 5% of SiO_2-MPS and 5% of SiO_2-Pol.

Structure	^{13}C chemical shift (ppm)			
	XNBR	NX 5%-SiO_2-MPS	NX 5%-SiO_2	NX 5%-SiO_2-Pol
$CH_3—(CH_2)10—CH_2OSO_3Na$[a]	14.8	14.8	14.8	14.8
B1A	22.0/23.7	23.7/24.6	23.7/24.6	24.6
A1, B4A	–	28.3	28.1	28.3
BB1	32.9	33.2	33.2	33.2
A2B	44.1	44.1	44.1	44.1
V2A	46.4	46.2	46.4	46.6
$CH_3—(CH_2)10—CH_2—OSO_3Na$[a]	–	69.3	69.1	69.1
V4V	116.0	115.0	–	114.8
AB3A	–	–	127.3	–
BB3B	130.8	130.8	130.8	130.8
V3A	143.1	142.9	142.4	143.6

[a] Surfactant.

Nanocomposites were also characterized by dynamic-mechanical analysis (DMA), as shown in Fig. 5 the elastic and plastic deformation responses, known as storage modulus (E') and loss modulus (E''), respectively. The value of tan δ (ratio of E''/E') can be understood as the damping behavior related to molecular mobility transitions, such as that occurs during the glass transition temperature (T_g). The Fig. 5a shows a pronounced decay of E' in the T_g range between −40 and −20 °C for all samples [35]. The temperature of this transition is easily observed in the maximum intensity of the curves of E'' (Fig. 5b). It may be noted that all nanocomposites have lower elastic and plastic deformation than the pure XNBR, possibly due to the domains formed in the presence of nanoparticles, which is in good agreement with the solid-state ^{13}C NMR analyses. In addition, nanoparticles reduced the number of hydrogen bonds that are responsible for the enhanced mechanical properties of pure XNBR [36,37].

The T_g of the nanocomposites barely changed, even for samples varying the amounts of nanoparticles with different surfaces (Table 3). Although their modified local mobility, the nanocomposites exhibited similar stiffness. Correlating the DMA results with the $T_{1\rho}$ values, the higher mechanical behavior of pure XNBR can be related to the stronger intermolecular and intramolecular interactions among their polymeric chains. On the other hand, the addition of SiO_2-Pol, which were poorly dispersed in the polymeric matrix and enhanced local mobility of the macromolecules, reduced mechanical performance of the nanocomposites. Although the presence of the MPS coupling agent resulted in an enhanced E' in the glassy state, indicating a better interaction between the inorganic/organic phase, both modified SiO_2-MPS and unmodified SiO_2 nanoparticles exhibited the same trend of $T_{1\rho}$ values and mechanical properties.

The loss modulus curves in Fig. 5b are related to the viscous dissipation portion and the full width at half maximum (FWHM) of the peaks in Table 3 is related to the relaxation of the chain segments and can be broadened by the presence of heterogeneities in nanocomposites [38,39]. Theoretical studies showed that highly interconnected systems exhibit a decrease in the intensity of peak of E'' combined with an enlargement of the FWHM [39,40]. Composites with weak interaction between the components interface present more intense peaks of loss modulus, while an improved interfacial adhesion results in lower intensities with

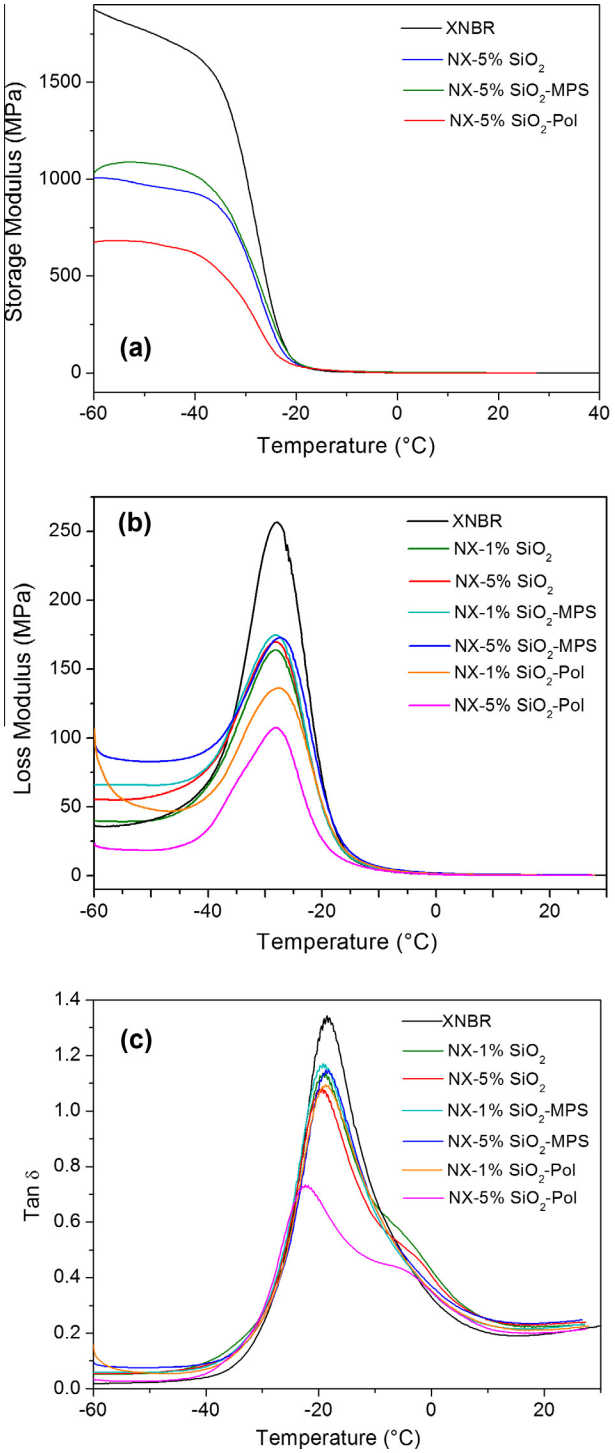

Fig. 5. Storage modulus (a), loss modulus (b) and tan δ (c) of pure polymer and nanocomposites with 1% and 5% of SiO_2, SiO_2-MPS and SiO_2-Pol. The pronounced decay or peak intensity of the graphs occur during the glass transition temperature.

Table 3
Dynamic-mechanical properties calculated for the XNBR and nanocomposites with SiO_2, SiO_2-MPS and SiO_2-Pol.

Samples	T_g (°C)	$(Ea)_{avg}$ (kJ/mol)	FWHM (°C)
XNBR	−27.7	285.5	11.9
NX-1%SiO_2	−26.9	167.3	13.5
NX-5%SiO_2	−27.3	218.1	13.1
NX-1%SiO_2-MPS	−27.1	230.9	12.7
NX-5%SiO_2-MPS	−26.1	213.8	12.9
NX-1%SiO_2-Pol	−28.5	242.9	13.6
NX-5%SiO_2-Pol	−28.0	258.4	12.6

reduced energy dissipation [17,39]. The average activation energy of the relaxation process $(Ea)_{avg}$ is relate to the extent of damping and molecular architecture and was calculated from the area under the loss modulus curve (Table 3) [41]. Lower $(Ea)_{avg}$ means that less energy is necessary for the relaxation process during the glass transition in nanocomposites because their heterogeneities increased the local mobility and facilitated the initial movement of some segments of the polymer backbone [18].

In this sense, we could show that using solid-state NMR analysis to investigate the dynamics of nanocomposites structure can predict the mechanical properties of hybrid materials. More than that, this technique could study how a material made of the same inorganic particles and organic polymer matrix can have distinctively morphological and structural features by changing the interface components, and precisely determine the final mechanical behavior.

4. Conclusions

We were able to identify how silica nanoparticles with different modified surface (MPS silane agent and a polymer shell of styrene–divinylbenzene) interacted with a typical latex elastomer and posteriorly define the mechanical behavior of nanocomposites. Using solid-state NMR we could prove the saturated carbons from XNBR underwent a marked change in the presence of nanoparticles and not the functional groups with unsaturated carbons, which are usually believed to interact with nanoparticles. Modifying the dynamics structure of the XNBR saturated region with the presence of SiO_2 predetermined the next mechanical properties observed. In this sense, the SiO_2-Pol which has the most hydrophobic surface, showed the highest value of $T_{1\rho}$ because it was not so well dispersed in the XNBR matrix and reduced the dynamic-mechanical properties of the nanocomposite. On the other hand, the SiO_2-MPS and bare SiO_2 nanoparticles, which have more hydrophilic surface presented similar $T_{1\rho}$ and mechanical properties, indicating similar macro arrangements of the polymer chains around these nanoparticles. Therefore solid-state NMR showed to be a great technique to investigate the role played by inorganic particles and the organic polymer matrix in a nanocomposite system, which will determine the mechanical properties and the application of these nanomaterials.

Acknowledgments

The financial support of FAPESP (Grants 2012/07067-0 and 2012/05013-0), CNPq, CAPES is gratefully acknowledged. We also acknowledge the support of CEPID/CDMF (FAPESP 2013/07296-2) and Nitriflex.

Appendix A. Supplementary material

Supplementary data associated with this article can be found, in the online version, at http://dx.doi.org/10.1016/j.jcis.2015.12.028.

References

[1] T.A. Vilgis, G. Heinrich, Reinforcement of Polymer Nano-Composites: Theory, Experiments and Applications, Cambridge University Press, 2009.
[2] F. Bauer, H. Ernst, U. Decker, M. Findeisen, H.-J. Gläsel, H. Langguth, et al., Preparation of scratch and abrasion resistant polymeric nanocomposites by monomer grafting onto nanoparticles, 1 FTIR and multi-nuclear NMR spectroscopy to the characterization of methacryl grafting, Macromol. Chem. Phys. 201 (18) (2000) 2654–2659.
[3] T. Kashiwagi, A.B. Morgan, J.M. Antonucci, M.R. VanLandingham, R.H. Harris, W.H. Awad, J.R. Shields, Thermal and flammability properties of a silica-poly (methylmethacrylate) nanocomposite, J. Appl. Polym. Sci. 89 (2003) 2072–2078.
[4] Y.-Y. Yu, C.-Y. Chen, W.-C. Chen, Synthesis and characterization of organic–inorganic hybrid thin films from poly(acrylic) and monodispersed colloidal silica, Polymer 44 (3) (2003) 593–601.
[5] Y. Sun, Z. Zhang, C.P. Wong, Influence of interphase and moisture on the dielectric spectroscopy of epoxy/silica composites, Polymer 46 (7) (2005) 2297–2305.
[6] Y.-l. Su, Preparation of polydiacetylene/silica nanocomposite for use as a chemosensor, React. Funct. Polym. 66 (9) (2006) 967–973.
[7] I.I. Slowing, J.L. Vivero-Escoto, C.-W. Wu, V.S.Y. Lin, Mesoporous silica nanoparticles as controlled release drug delivery and gene transfection carriers, Adv. Drug Del. Rev. 60 (11) (2008) 1278–1288.
[8] J.H. Kang, E.J. Siochi, R.K. Penner, T.L. Turner, Enhanced adhesive strength between shape memory polymer nanocomposite and titanium alloy, Compos. Sci. Technol. 96 (2014) 23–30.
[9] W.Y.D. Yong, Z. Zhang, G. Cristobal, W.S. Chin, One-pot synthesis of surface functionalized spherical silica particles, Colloids Surf. Physicochem. Eng. Aspects (2014).
[10] Y. Jiao, J. Parra, P. Akcora, Effect of ionic groups on polymer-grafted magnetic nanoparticle assemblies, Macromolecules 47 (6) (2014) 2030–2036.
[11] A. Mousa, G. Heinrich, F. Simon, U. Wagenknecht, K.-W. Stöckelhuber, R. Dweiri, Carboxylated nitrile butadiene rubber/hybrid filler composites, Mater. Res. 15 (4) (2012) 671–678.
[12] H. Kang, K. Zuo, Z. Wang, L. Zhang, L. Liu, B. Guo, Using a green method to develop graphene oxide/elastomers nanocomposites with combination of high barrier and mechanical performance, Compos. Sci. Technol. 92 (2014) 1–8.
[13] M. Prochoń, A. Przepiórkowska, M. Zaborski, Keratin as a filler for carboxylated acrylonitrile-butadiene rubber XNBR, J. Appl. Polym. Sci. 106 (6) (2007) 3674–3687.
[14] P.A. Steward, J. Hearn, M.C. Wilkinson, An overview of polymer latex film formation and properties, Adv. Colloid Interface Sci. 86 (3) (2000) 195–267.
[15] W. Hu, Y. Su, L. Zhou, A. Pang, R. Cai, X. Ma, et al., Molecular dynamics of neutral polymer bonding agent (NPBA) as revealed by solid-state NMR spectroscopy, Molecules 19 (1) (2014) 1353–1366.
[16] R. Nogueira, M. Tavares, A. Ferreira, The use of multinuclear solid-state NMR to evaluate polystyrene/silica composites, J. Nanopart. Res. 14 (8) (2012) 1–8.
[17] W. Kolodziejski, J. Klinowski, Kinetics of cross-polarization in solid-state NMR: a guide for chemists, Chem. Rev. 102 (3) (2002) 613–628.
[18] H.L. Ornaghi, A.S. Bolner, R. Fiorio, A.J. Zattera, S.C. Amico, Mechanical and dynamic mechanical analysis of hybrid composites molded by resin transfer molding, J. Appl. Polym. Sci. 118 (2) (2010) 887–896.
[19] W. Stöber, A. Fink, E. Bohn, Controlled growth of monodisperse silica spheres in the micron size range, J. Colloid Interface Sci. 26 (1) (1968) 62–69.
[20] R.L. Sala, T.M. Arantes, E. Longo, E.R. Leite, C.M. Paranhos, E.R. Camargo, Evaluation of modified silica nanoparticles in carboxylated nitrile rubber nanocomposites, Colloids Surf. Physicochem. Eng. Aspects 462 (2014) 45–51.
[21] J. Zhang, J. Yang, Q. Wu, M. Wu, N. Liu, Z. Jin, et al., SiO_2/polymer hybrid hollow microspheres via double in situ miniemulsion polymerization, Macromolecules 43 (3) (2010) 1188–1190.
[22] S. Borsacchi, M. Geppi, C.A. Veracini, F. Fallani, L. Ricci, G. Ruggeri, Improving compatibility in LDPE-silica dispersions by photo-grafting reaction. Preparation and solid state NMR investigation, J. Mater. Chem. 16 (47) (2006) 4581.
[23] R.V. Law, D.C. Sherrington, C.E. Snape, Quantitative solid state ^{13}C NMR studies of highly cross-linked poly(divinylbenzene) resins, Macromolecules 30 (10) (1997) 2868–2875.
[24] K. Landfester, N. Bechthold, F. Tiarks, M. Antonietti, Miniemulsion polymerization with cationic and nonionic surfactants: a very efficient use of surfactants for heterophase polymerization, Macromolecules 32 (8) (1999) 2679–2683.
[25] D.J.T. Hill, J.H. O'Donnell, M.C.S. Perera, P.J. Pomery, An investigation of radiation-induced structural changes in nitrile rubber, J. Polym. Sci., Part A: Polym. Chem. 34 (12) (1996) 2439–2454.
[26] D.C. Apperley, R.K. Harris, P. Hodgkinson, Solid State NMR: Basic Principles and Practice, Momentum Press, 2012.
[27] T.M. Arantes, K.V. Leão, M.I.B. Tavares, A.G. Ferreira, E. Longo, E.R. Camargo, NMR study of styrene-butadiene rubber (SBR) and TiO_2 nanocomposites, Polym. Test 28 (5) (2009) 490–494.
[28] A.A. Passos, M.I.B. Tavares, R.C.P. Neto, L.A. Moreira, A.G. Ferreira, Obtenção de nanocompósito de EVA/sílica e caracterização por ressonância magnética nuclear no estado sólido, Polímeros 21 (2011) 98–102.
[29] T.E. Motaung, M.L. Saladino, A.S. Luyt, D.F. Chillura Martino, The effect of silica nanoparticles on the morphology, mechanical properties and thermal degradation kinetics of polycarbonate, Compos. Sci. Technol. 73 (2012) 34–39.

[30] M.L. Saladino, T.E. Motaung, A.S. Luyt, A. Spinella, G. Nasillo, E. Caponetti, The effect of silica nanoparticles on the morphology, mechanical properties and thermal degradation kinetics of PMMA, Polym. Degrad. Stab. 97 (3) (2012) 452–459.
[31] R. Shenhar, T.B. Norsten, V.M. Rotello, Polymer-mediated nanoparticle assembly: structural control and applications, Adv. Mater. 17 (6) (2005) 657–669.
[32] H. Zou, S. Wu, J. Shen, Polymer/silica nanocomposites: preparation, characterization, properties, and applications, Chem. Rev. 108 (9) (2008) 3893–3957.
[33] Y.-L. Liu, C.-Y. Hsu, K.-Y. Hsu, Poly(methylmethacrylate)-silica nanocomposites films from surface-functionalized silica nanoparticles, Polymer 46 (6) (2005) 1851–1856.
[34] H. Liu, T. Wang, Q. Wang, In situ synthesis and properties of PMR PI/SiO_2 nanocomposites, J. Appl. Polym. Sci. 125 (1) (2012) 488–493.
[35] S.N. Cassu, M.I. Felisberti, Comportamento dinâmico-mecânico e relaxações em polímeros e blendas poliméricas, Quim Nova 28 (2005) 255–263.
[36] J. Pietrasik, M. Gaca, M. Zaborski, L. Okrasa, G. Boiteux, O. Gain, Studies of molecular dynamics of carboxylated acrylonitrile-butadiene rubber composites containing in situ synthesized silica particles, Eur. Polym. J. 45 (12) (2009) 3317–3325.
[37] M. Preghenella, A. Pegoretti, C. Migliaresi, Thermo-mechanical characterization of fumed silica-epoxy nanocomposites, Polymer 46 (26) (2005) 12065–12072.
[38] S.Y. Soong, R.E. Cohen, M.C. Boyce, Polyhedral oligomeric silsesquioxane as a novel plasticizer for poly(vinyl chloride), Polymer 48 (5) (2007) 1410–1418.
[39] S. Kumar, B. Satapathy, A. Patnaik, Viscoelastic interpretations of erosion performance of short aramid fibre reinforced vinyl ester resin composites, J. Mater. Sci. 46 (23) (2011) 7489–7500.
[40] J.J. La Scala, M.S. Logan, J.M. Sands, G.R. Palmese, Composites based on bimodal vinyl ester resins with low hazardous air pollutant contents, Compos. Sci. Technol. 68 (7–8) (2008) 1869–1876.
[41] M.C.O. Chang, D.A. Thomas, L.H. Sperling, Characterization of the area under loss modulus and tan δ–temperature curves: acrylic polymers and their sequential interpenetrating polymer networks, J. Appl. Polym. Sci. 34 (1) (1987) 409–422.